Supplementary Information

Ngfr^{+} cholinergic projection from SI/nBM to mPFC selectively regulates temporal order recognition memory

Supplementary Fig.1

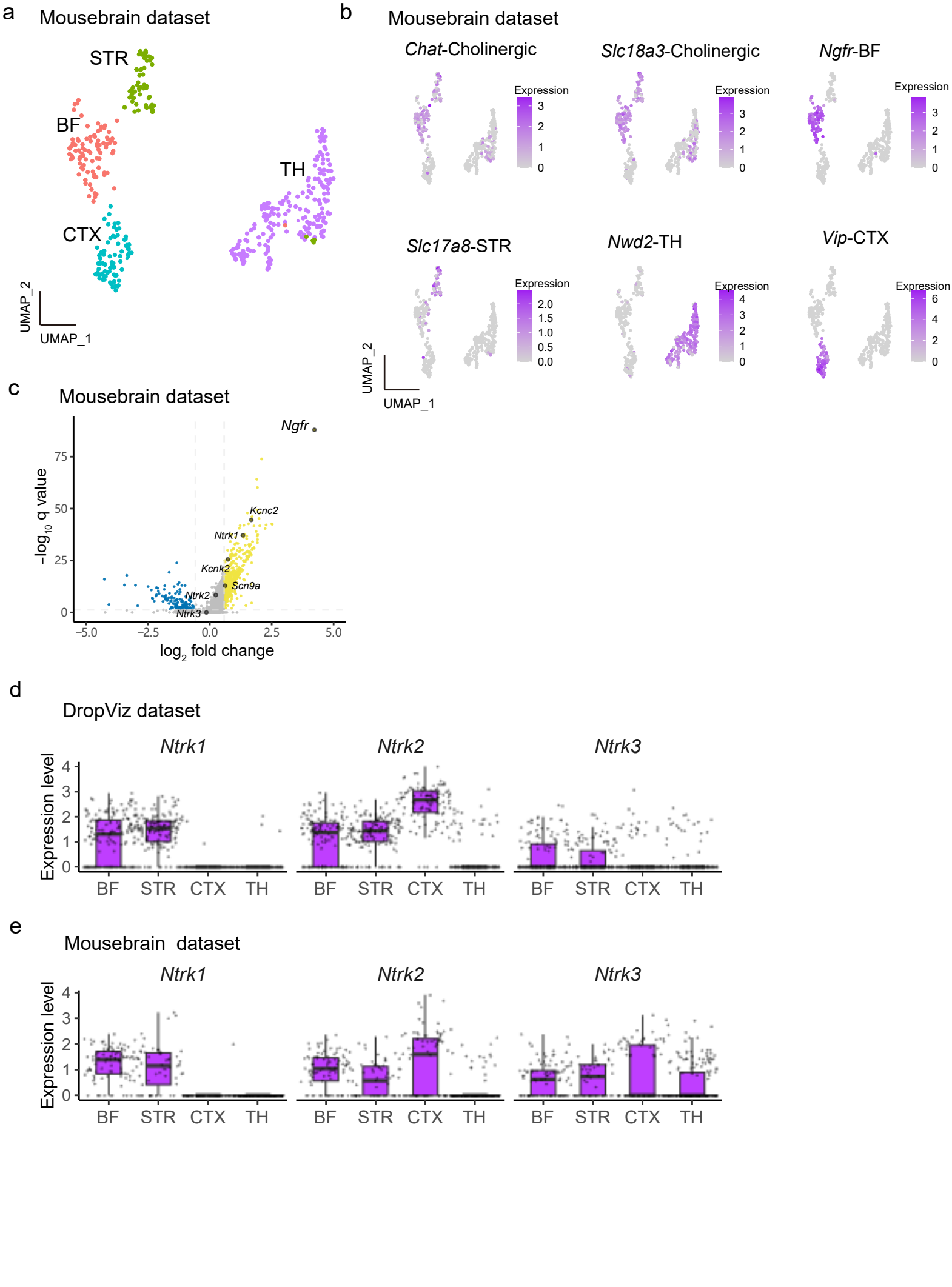

Supplementary Fig. 1. *Ngfr* specifically labels cholinergic projection neurons in BF

(a) Cholinergic neurons from different anatomic boundaries are clustered using UMAP (based on the Mousebrain dataset). Numbers of *Chat*$^{+}$ cholinergic neuron sampled are indicated. BF, n=89 cells; STR, n=62 cells; CTX, n=80 cells; TH, n= 204 cells.

(b) Visualization of each cholinergic cluster using specific marker genes in UMAP. Cholinergic, *Chat* and *Slc18a3*; Basal forebrain, *Ngfr*; Striatum, *Slc17a8*; Thalamus, *Nwd2*; Cortex, *Vip*.

(c) Volcano plot showing the DEGs that differentiate the BF cholinergic projection neurons from the other cholinergic clusters, based on the Mousebrain dataset. Top DEGs are highlighted ($\log_2$ fold change>1, q<0.05). $\log_2$ fold change>1 indicates genes enriched in the BF cholinergic neurons.

(d) Gene expression levels of neurotrophic factors in BF, STR, CTX and TH, as normalized by total UMIs with scaling factor of 10000 and log transformed (logTP10K, tags per 10K UMIs). The data is from the DropViz dataset.

(e) Relative expression of neurotrophic factors in BF, STR, CTX and TH in logTP10K. The expression data is based on the Mousebrain dataset.

Statistical analyses in (c) were performed by two-sided wilcox test, p value adjusted by FDR to get q value.

Supplementary Fig. 2

a

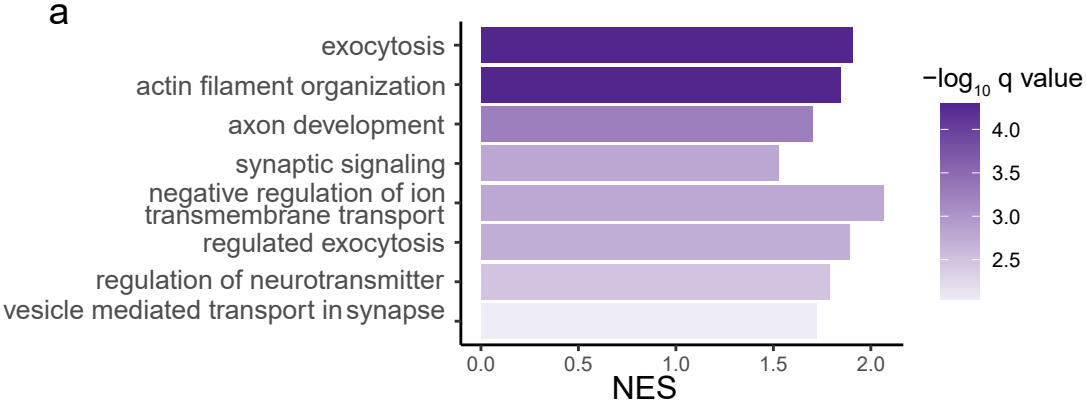

b

Cholinergic neuron with GFP

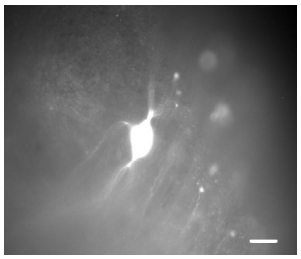

c

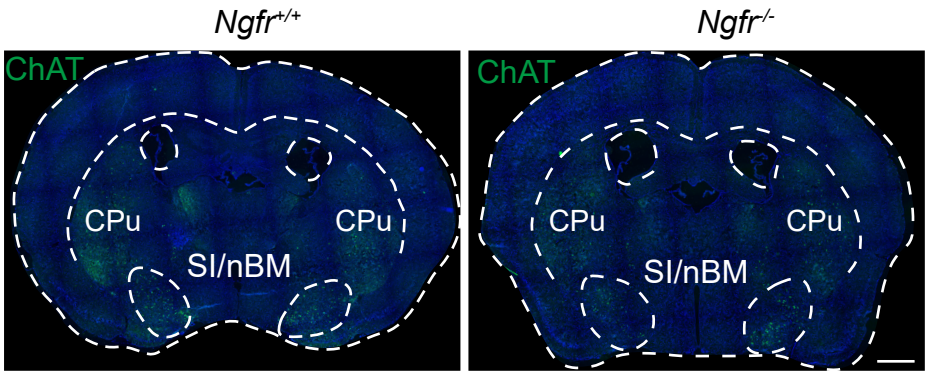

d

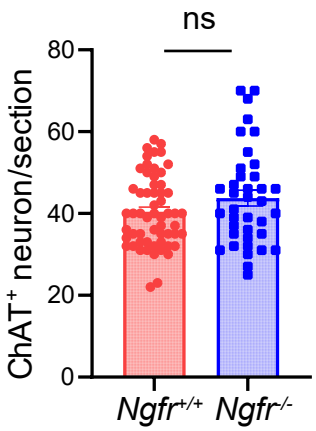

Supplementary Fig. 2. NGFR functionally correlates with synaptic regulation

(a) Gene set enrichment analysis (GSEA) of gene expression profiles of BF cholinergic projection neurons versus cholinergic clusters from the other brain regions, based on the Mousebrain database. The GO database was used for the annotation of biological process. q values for each pathway are determined by FDR.

(b) Representative image of cholinergic neuron with GFP. Scale bar, 20 μm.

(c) Representative images of immunofluorescence staining of $ChAT^+$ cholinergic neurons in adult *Ngfr*$^{+/+}$ and *Ngfr*$^{-/-}$ mice. Scale bar, 1 mm.

(d) No significant difference in the cell number of $ChAT^+$ cholinergic neurons in the SI/nBM from adult *Ngfr*$^{+/+}$ and *Ngfr*$^{-/-}$ mice. p=0.12. *Ngfr*$^{+/+}$, n=58 sections from 6 mice; *Ngfr*$^{-/-}$, n=38 sections from 8 mice.

Numerical data are means ± SEM. Statistical analyses were performed by unpaired two-sided t test in (d). Source data are provided as a Source Data file.

Supplementary Fig. 3

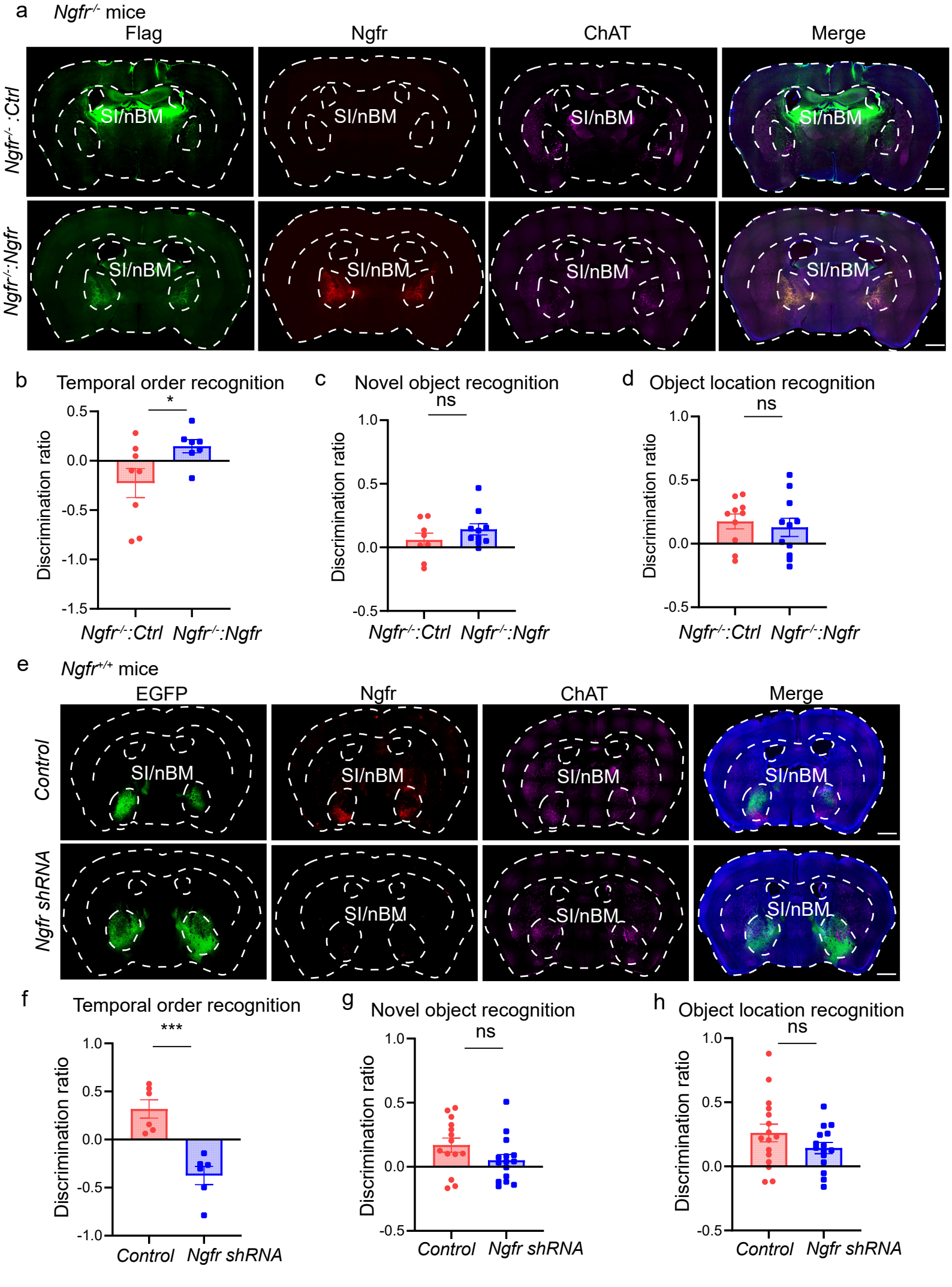

Supplementary Fig. 3. *Ngfr* expression in SI/nBM controls temporal order recognition memory

(a) Immunofluorescence staining revealed significant NGFR immunoreactivity in SI/nBM but not in other regions by AAV infection (bottom row), indicating re-expression of NGFR in the cholinergic neurons of *Ngfr*$^{-/-}$ mice at ages of 2 to 5 months. Scale bar, 1 mm.

(b) *Ngfr* expression rescued impairment in temporal order recognition in *Ngfr*$^{-/-}$ mice. p=0.045. *Ngfr*$^{-/-}$*:Ctrl*, n=8; *Ngfr*$^{-/-}$*:Ngfr*, n=7.

(c) No significant changes in novel object recognition by *Ngfr* expression in *Ngfr*$^{-/-}$ SI/nBM. p=0.24. *Ngfr*$^{-/-}$*:Ctrl*, n=8; *Ngfr*$^{-/-}$*:Ngfr*, n=10.

(d) No significant difference in object location recognition by *Ngfr* expression in *Ngfr*$^{-/-}$ mice. p=0.63. *Ngfr*$^{-/-}$*:Ctrl*, n=10; *Ngfr*$^{-/-}$*:Ngfr*, n=11.

(e) Immunofluorescence revealed a marked reduction in *Ngfr* expression in SI/nBM cholinergic neurons by *Ngfr* shRNA in the wild-type at ages of 2 to 3 months. Scale bar, 1 mm.

(f) Reduction in *Ngfr* expression in SI/nBM significantly impaired temporal order recognition memory in wild-type mice. p=0.0004. *Control*, n=6; *Ngfr shRNA*, n=6.

(g) No significant changes in novel object recognition by reduced *Ngfr* expression in wild-type SI/nBM. p=0.11. *Control*, n=14; *Ngfr shRNA*, n=15.

(h) No significant difference in object location recognition by reduced *Ngfr* expression in wild-type SI/nBM. p=0.16. *Control*, n=16; *Ngfr shRNA*, n=15.

Numerical data are means ± SEM. Statistical analyses were performed by unpaired two-sided t test in (b), (c), (d), (f), (g) and (h). Source data are provided as a Source Data file.

Supplementary Fig. 4

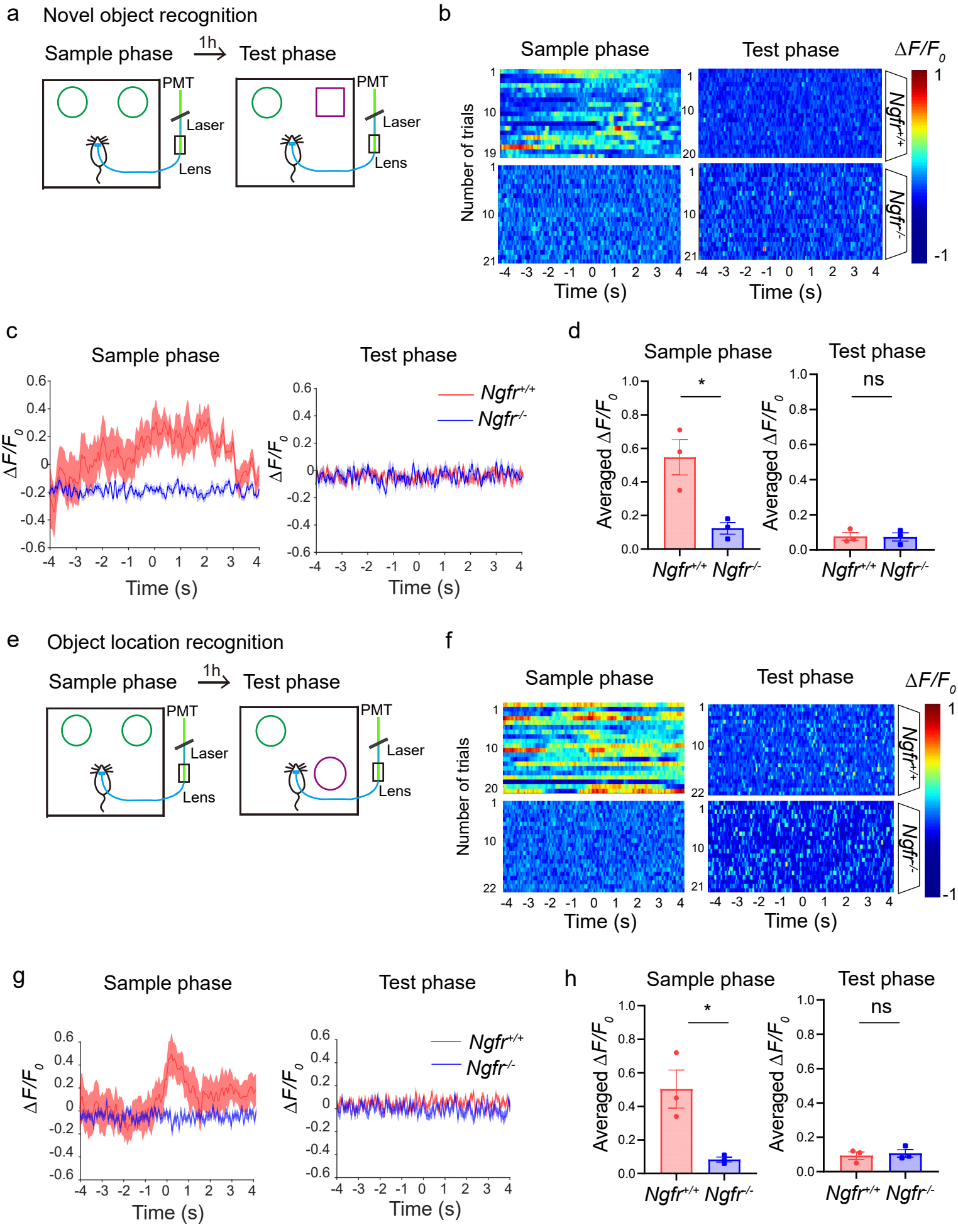

Supplementary Fig. 4. ACh release in mPFC during novel object and object location recognition memory task

(a) Schematic diagram depicting the measurement of relative ACh levels by a fluorescent ACh3.0 sensor during the sample and test phase in novel object recognition.

(b) Pseudocolored fluorescence responses of ACh3.0 in mPFC during object encounters (time 0) in the sample and test phase of novel object recognition. Color scale indicates $\Delta F/F_0$. ACh signals detected in the wild-type mice during the sample phase but not test phase.

(c) Averaged ACh release upon object encounters. Phasic ACh release was absent in *Ngfr*$^{-/-}$ mice. Thick lines indicate the averaged values between trials and the shaded areas represent SEM.

(d) Group summary of peak ACh signals indicated ACh release in the sample phase in *Ngfr*$^{+/+}$ mice but not in *Ngfr*$^{-/-}$ mice. Sample phase, p=0.019; Test phase, p=0.92. *Ngfr*$^{+/+}$, n=3; *Ngfr*$^{-/-}$, n=3.

(e) Schematic diagram showing the measurement of ACh dynamics in the sample and test phase of object location recognition.

(f) Pseudocolored ACh signals in mPFC during object encounters (time 0) in the sample and test phase of object location recognition. Color scale indicates $\Delta F/F_0$. ACh signals detected in the wild-type mice during the sample phase but not test phase.

(g) Averaged ACh release upon object encounters in object location memory test. ACh release was absent in *Ngfr*$^{-/-}$ mice. Thick lines indicate the averaged values between trials and the shaded areas represent SEM.

(h) Group summary of peak ACh signals indicated ACh release only in the sample phase in wild-type mice during object location recognition. Sample phase, p=0.021; Test phase, p=0.69. *Ngfr*$^{+/+}$, n=3; *Ngfr*$^{-/-}$, n=3.

Statistical analyses were performed by unpaired two-sided t test in (d) and (h). Source data are provided as a Source Data file.

Supplementary Fig. 5

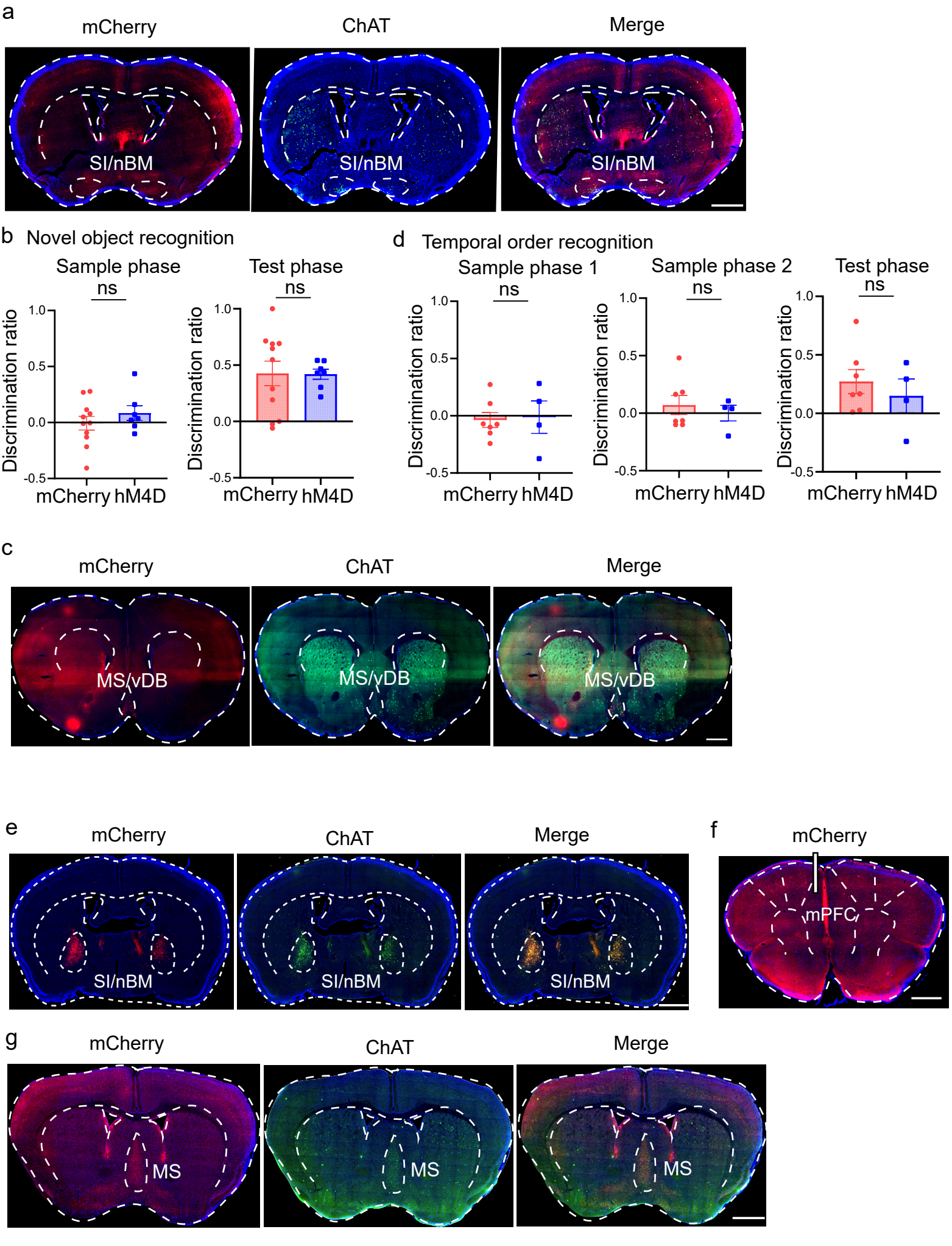

Supplementary Fig. 5. Chemogenetic and optogenetic inhibition of cholinergic innervation in ChAT-Cre mice

(a) Fluorescence signals of retrogradely transported Cre-dependent hM4D-mCherry AAV-Retro virus from mPFC to SI/nBM cholinergic neurons as indicated by immunofluorescence staining of ChAT in ChAT-Cre mice. Scale bar, 1 mm.

(b) No significant changes in novel object recognition by chemogenetic inhibition of SI/nBM-mPFC cholinergic circuitry. Sample phase, p=0.34; Test phase, p=0.96. mCherry, n=11; hM4D, n=7.

(c) Expression of Cre-dependent hM4D-mCherry AAV9 in MS/vDB in ChAT-Cre mice. Scale bar, 1 mm.

(d) No significant changes in temporal order recognition by chemogenetic inhibition of MS/vDB cholinergic neurons. Sample phase 1, p=0.86; Sample phase 2, p=0.58; Test phase, p=0.50. mCherry, n=7; hM4D, n=4.

(e-f) Expression of eNpHR3.0-mCherry virus in the SI/nBM cholinergic neurons as indicated by immunofluorescence staining of ChAT (e). eNpHR3.0-mCherry-expressing cholinergic terminals in the mPFC of ChAT-Cre mice (f). Scale bar, 1 mm.

(g) Fluorescence of retrogradely transported Cre-dependent hM4D-mCherry AAV-Retro virus from HP to MS cholinergic neuron as indicated by immunofluorescence of ChAT in ChAT-Cre mice. Scale bar, 1 mm.

Statistical analyses were performed by unpaired two-sided t test in (b) and (d). Source data are provided as a Source Data file.

Supplementary Fig. 6

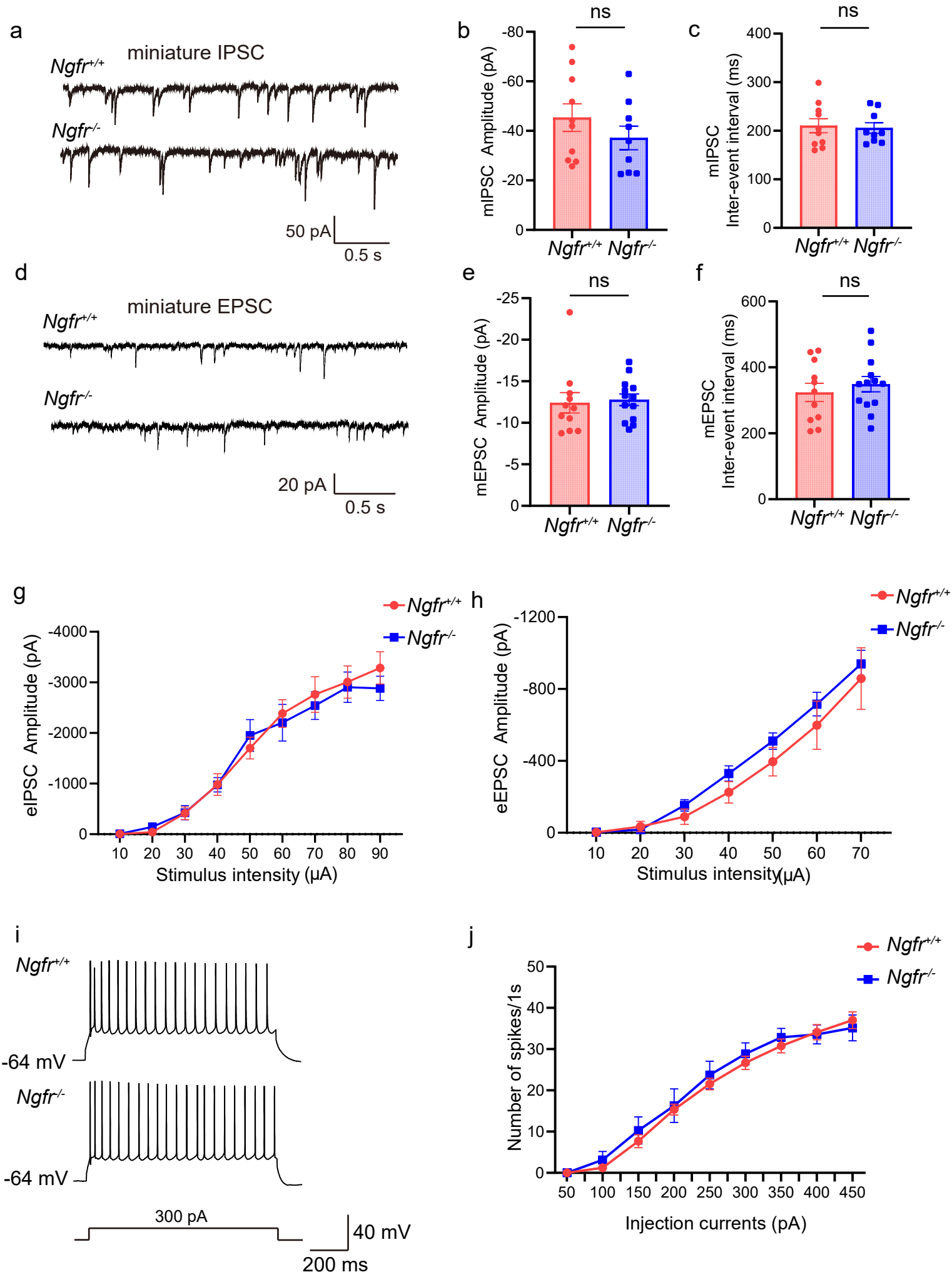

Supplementary Fig. 6. Synaptic transmission and neuron excitability of mPFC layer V pyramidal neuron

(a) Example traces of miniature IPSCs (mIPSCs) of pyramidal neurons in mPFC layer V, by whole-cell patch recordings at a holding potential of -70 mV, in the presence of 1.5 μM TTX, 50 μM APV and 50 μM CNQX.

(b-c) No significant difference in amplitude (p=0.28) or inter-event interval (p=0.80) of mIPSCs between *Ngfr*$^{+/+}$ and *Ngfr*$^{-/-}$ mice. *Ngfr*$^{+/+}$, n=10 cells from 5 mice; *Ngfr*$^{-/-}$, n=9 cells from 3 mice.

(d) Example traces of miniature EPSCs (mEPSCs), recorded by whole-cell patch in the presence of 1.5 μM TTX and 80 μM picrotoxin.

(e-f) Quantification of mEPSCs shows no difference in amplitude (p=0.79) or inter-event interval (p=0.49) between genotypes. *Ngfr*$^{+/+}$, n=11 cells from 3 mice; *Ngfr*$^{-/-}$, n=13 cells from 3 mice.

(g) Evoked IPSCs (eIPSCs) were induced by extracellular stimulation at layer II/III of mPFC at a holding potential of -70 mV, in the presence of 50 μM APV and 50 μM CNQX. No significant difference in eIPSCs amplitude in response to a number of different stimulus intensities between genotypes. $F_{interaction}(8,136)=0.63$, $p=0.75$; $F_{stimulus}(2.08,35.41)=106.2$, $p<0.0001$; $F_{genotype}(1,17)=0.059$, $p=0.81$. *Ngfr*$^{+/+}$, n=10 cells from 5 mice; *Ngfr*$^{-/-}$, n=9 cells from 5 mice.

(h) Evoked EPSCs (eEPSCs) were induced by extracellular stimulation at the layer II/III of the mPFC at a holding potential of -70 mV, in the presence of 80 μM picrotoxin. eEPSCs amplitude in response to a series of different stimulus intensities is similar between genotypes. $F_{interaction}(6,90)=0.57$, $p=0.75$; $F_{stimulus}(1.26,18.95)=87.99$, $p<0.0001$; $F_{genotype}(1,15)=0.81$, $p=0.38$. *Ngfr*$^{+/+}$, n=8 cells from 4 mice; *Ngfr*$^{-/-}$, n=9 cells from 4 mice.

(i) Representative traces of action potential discharges evoked by long depolarization pulse (300 pA, 1s) in the mPFC layer V pyramidal neurons from *Ngfr*$^{+/+}$ and *Ngfr*$^{-/-}$ mice.

(j) Intact excitability of mPFC layer V pyramidal neurons from *Ngfr*$^{-/-}$ mice. Numbers of action potential were plotted against the depolarizing currents injected into the pyramidal neurons. $F_{interaction}(8,112)=0.53$, $p=0.84$; $F_{currents}(1.89,26.41)=168.3$, $p<0.0001$; $F_{genotype}(1,14)=0.24$, $p=0.64$. *Ngfr*$^{+/+}$, n=9 cells from 5 mice; *Ngfr*$^{-/-}$, n=7 cells from 5 mice.

Numerical data are means ± SEM. Statistical analyses were performed by unpaired two-sided t test in (b), (c), (e) and (f), and two-way ANOVA with Bonferroni's multiple comparisons in (g), (h) and (j). Source data are provided as a Source Data file.

Supplementary Fig. 7

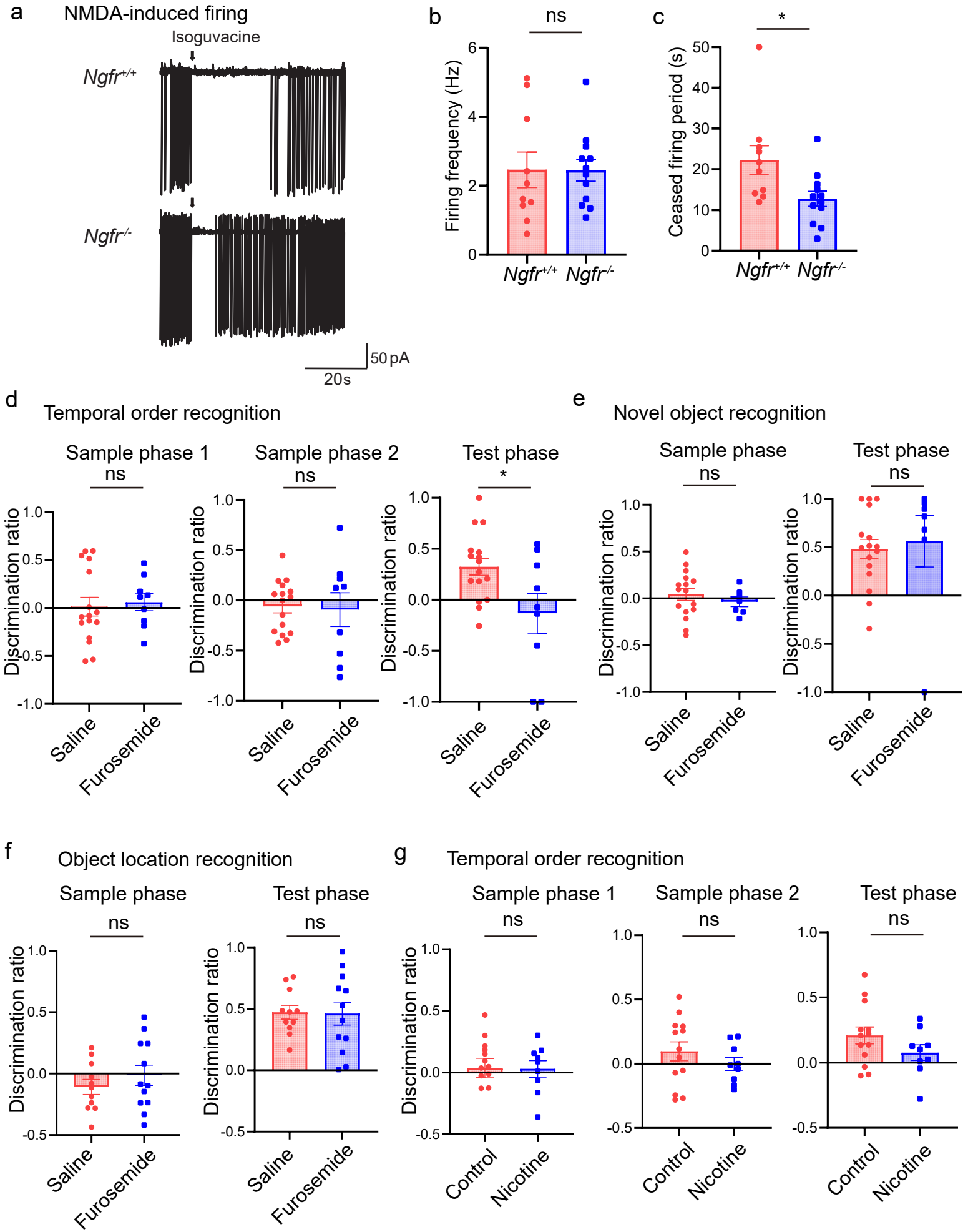

Supplementary Fig. 7. Effects of furosemide or nicotine treatment on recognition memory
(a) Cell-attached recordings of NMDA-induced firing. Representative traces of basal spike frequency and effects of puffing GABA agonist isoguvacine (100μM) on cortical inhibition.
(b) In steady-state, 12 μM NMDA-induced firing frequency in *Ngfr*$^{-/-}$ mice was similar with that in *Ngfr*$^{+/+}$ mice. p=0.98. *Ngfr*$^{+/+}$, n=10 cells from 3 mice; *Ngfr*$^{-/-}$, n=12 cells from 4 mice.
(c) After puffing isoguvacine, ceased firing period was significantly shorter in *Ngfr*$^{-/-}$ mice than that in *Ngfr*$^{+/+}$ mice. p=0.021. *Ngfr*$^{+/+}$, n=10 cells from 3 mice; *Ngfr*$^{-/-}$, n=12 cells from 4 mice.
(d) Delivery of 2mM furosemide in the mPFC by cannula significantly attenuated temporal order recognition in wild-type mice. Sample phase 1, p=0.76; Sample phase 2, p=0.83; Test phase, p=0.021. Saline, n=16; Furosemide, n=9.
(e) No significant difference in novel object recognition by delivery of 2mM furosemide in the wild-type mPFC. Sample phase, p=0.45; Test phase, p=0.73. Saline, n=16; Furosemide, n=7.
(f) Intact object location recognition by 2 mM furosemide delivery in the mPFC of wild-type mice. Sample phase, p=0.37; Test phase, p=0.93. Saline, n=11; Furosemide, n=12.
(g) No significant difference in temporal order recognition memory by chronic nicotine treatment over 4-week period in wild-type mice. Sample phase 1, p=0.95; Sample phase 2, p=0.34; Test phase, p=0.17. Control, n=13; Nicotine, n=9.
Numerical data are means ± SEM. Statistical analyses were performed by unpaired two-sided t test in (b), (c), (d), (e), (f) and (g). Source data are provided as a Source Data file.

SupplementaryTable 1

Membrane properties of cholinergic neuron in SI/nBM			
	Ngfr $^{+/+}$	*Ngfr* $^{-/-}$	p
Resting membrane potential (mV)	-61.8 ± 0.8	-62.5 ±0.7	0.52
Input resistance (GΩ)	0.6 ± 0.05	0.5 ± 0.05	0.06
Action potential threshold (mV)	-29.6 ± 0.8	-31.1 ± 0.6	0.06
Action potential amplitude (mV)	105.1 ± 4.2	111.6 ± 2.3	0.18
Action potential half-width (ms)	1.4 ± 0.1	1.3 ± 0.1	0.2

Membrane properties of cholinergic neuron in MS			
	Ngfr $^{+/+}$	*Ngfr* $^{-/-}$	p
Resting membrane potential (mV)	-61.8 ± 0.4	-62.2 ± 0.9	0.65
Input resistance (GΩ)	0.8 ± 0.1	0.6 ± 0.1	0.14
Action potential threshold (mV)	-30.1 ± 1.3	-31.1 ± 1.2	0.54
Action potential amplitude (mV)	109.1 ± 2.1	108.8 ± 3.1	0.93
Action potential half-width (ms)	1.8 ± 0.1	1.7 ± 0.1	0.77

Supplementary Table 1. No significant difference in membrane properties of cholinergic neurons in SI/nBM or MS between genotypes

Resting membrane potential, input resistance, action potential threshold, amplitude and half-width were measured. Intact membrane properties of SI/nBM or MS cholinergic neurons in *Ngfr*$^{-/-}$ mice. Action potential threshold was measured at the first point on the rising phase of the spike where the rate of rise exceeded 50 mV/ms.

Numerical data are means ± SEM. Statistical analyses were performed by unpaired two-sided t test. Source data are provided as a Source Data file.